KAERI/TR-3557/2008

기술보고서

증기폭발 혼합계산의 최적모델 및 모델인자 결정

DETERMINATION OF APPROPRIATE MODELS AND PARAMETERS FOR PREMIXING CALCULATIONS

2008 년 3 월

한국원자력연구원

Korea Atomic Energy Research Institute

제 출 문

한국원자력연구원장 귀하

본 보고서를 2008 년도 “노심용융물 위해도 실증실험 및 쟁점해결기술개발” 과제의 기술보고서로 제출합니다.

제목 : 증기폭발 혼합계산의 최적모델 및 모델인자 결정 (DETERMINATION OF APPROPRIATE MODELS AND PARAMETERS FOR PREMIXING CALCULATIONS)

2008 년 3 월

과제명: 노심용융물 위해도 실증실험 및 쟁점해결기술개발

주저자: 박익규
김종환
민병태
홍성완

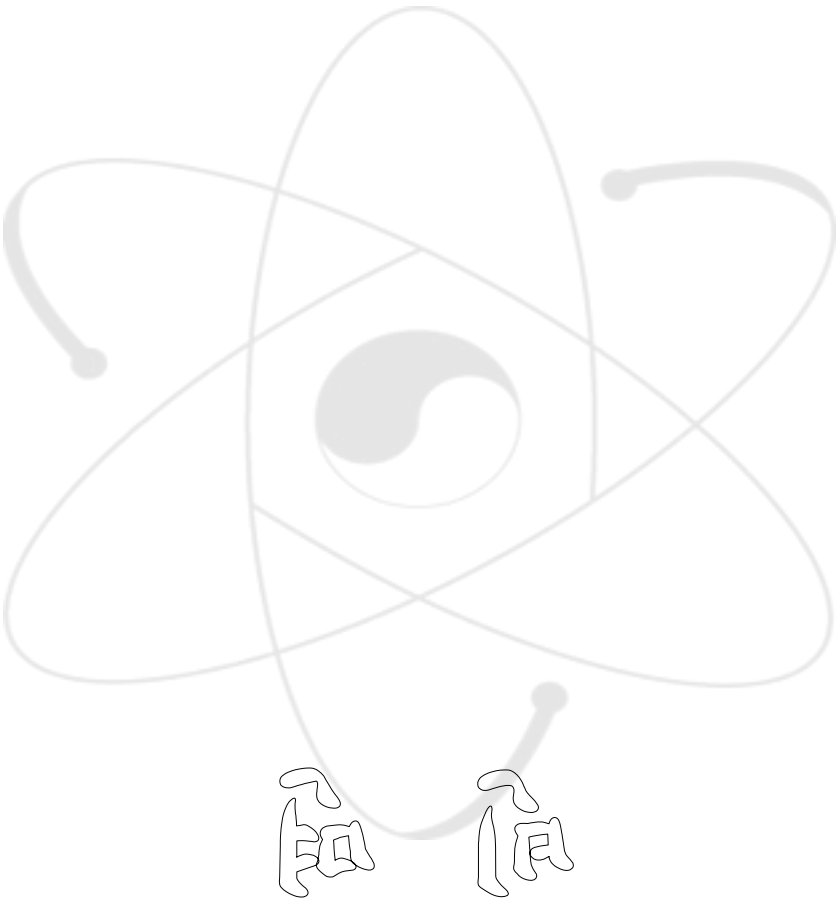

증기폭발 혼합계산의 최적모델 및 모델인자 결정

요 약 문

이 연구의 목적은 증기폭발의 혼합 계산에 있어서 가장 적절한 모델과 그 모델에 대한 모델인자를 도출하는 것이다. 이를 위하여 Forschungszentrum Karlsruhe 에서 수행된 실험을 증기폭발 해석코드인 MC3D 에 적용하였다.

QUEOS 실험 결과가 혼합단계에서 가장 적절한 열전달 모델을 찾고 이 모델에 대한 모델상수를 도출하기 위하여 사용되었다. QUEOS 실험은 작고 뜨거운 고체구를 사용하였기 때문에 특히 열전달 모델에 대한 검토용으로서 적합하다. 고체구는 용융물과는 달리 열전달 면적이 고정되어 있기 때문에 열전달 모델에 대한 타당성 검토가 특히 유리하다.

QUEOS 실험을 사용하여 열전달 모델 및 모델 상수를 고정한 뒤에 PREMIX 실험을 사용하여 혼합계산을 다시 수행하였다. PREMIX 실험은 코륨의 상사물로서 용융된 알루미나(Al_2O_3) 를 사용한 혼합실험이다. PREMIX 실험을 통하여서는 용융물 제트와 용융물 drop 에 대한 용융물 분쇄 모델에 대한 검토가 이루어졌다.

DETERMINATION OF APPROPRIATE MODELS AND PARAMETERS FOR PREMIXING CALCULATIONS

Summary

The purpose of the present work is to use experiments that have been performed at Forschungszentrum Karlsruhe during about the last ten years for determining the most appropriate models and parameters for premixing calculations.

The results of a QUEOS experiment are used to fix the parameters concerning heat transfer. The QUEOS experiments are especially suited for this purpose as they have been performed with small hot solid spheres. Therefore the area of heat exchange is known.

With the heat transfer parameters fixed in this way, a PREMIX experiment is recalculated. These experiments have been performed with molten alumina (Al_2O_3) as a simulant of corium. Its initial temperature is 2600 K. With these experiments the models and parameters for jet and drop break-up are tested.

목 차

표 목차

그림 목차

Jacobs, Helmut, Park Ik-kyu et al. 20 September 2007
KAERI/TROI

Dr. Jacobs who has worked for Forschungszentrum Karlsruhe has joined TROI team from April.25.2007 to September.24.2007 as Brain Pool Program of The Korean Federation of Science and Technology Societies.

Determination of Appropriate Models and Parameters for Premixing Calculations with the Steam Explosion Code MC3D

Outline

1. Introduction
2. The QUEOS experiments
    - General
    - Experiment Q58
    - Recalculation of Q58
3. The PREMIX experiments
    - General
    - The experiment PM18
    - Recalculation of PM18
4. Conclusions

1. Introduction

The code MC3D [1] was originally developed by CEA, France, and is owned by IRSN, France. It has been one of the first multi-fluid codes that have been developed for modeling the phenomena occurring when hot liquids are mixed with cold, more volatile liquids.

These involve break-up and quenching of the hot liquid, steam production, and possibly explosive vaporization, which is also called steam explosion. In the context of nuclear safety these phenomena are also called Fuel Coolant Interaction (FCI). Especially in this area the initial and boundary conditions are extreme and often lay outside the parameter range normally encountered in thermo- and fluid dynamics.

Above all, the molten core material, called the corium, is assumed to have a temperature of the order of 3000 K and as well its composition as its properties are quite uncertain. Also, there are a large number of phenomena that can play an important role, like

- Breakup of a continuous corium flow into individual particles (i.e. globules or droplets), which is mostly denoted as jet breakup;
- Further (slow) breakup of these droplets into smaller ones, but still in the centimeter or millimeter range;
- Extremely fast fine scale fragmentation of the drops to the 0.1-mm range (this is the process that makes explosions);
- Heat transfer from the hot melt to water in what is called film boiling which, however, under the given highly irregular and violent boundary conditions, may well involve local and transient direct liquid-liquid contact with spontaneous flashing of a water layer superheated beyond the limit of stability (the spontaneous nucleation temperature);
- Vaporization of the water due to the just described heat transfer;
- Pressure development due to temperature rise and vapor generation;
- Fluid motion due to the so developed steep pressure gradients;
- Heat transfer from the extremely small fragments to a fast moving two-phase water environment at subcritical and supercritical pressures.
- Momentum exchange (drag) between the phases.

Many of these processes are not fully understood which is especially true for the exotic parameter range encountered in nuclear safety problems. Therefore the developers of MC3D have incorporated into their code a variety of models for the most important phenomena and, in addition, have provided these models with free parameters so that they can be adjusted to relevant experimental observations as they become available.

Alls calculations of this work have been performed with the version 3.5 patch1. The code also contains an option to treat solid spheres that do not change their size. This option has been used in one of the cases below.

The purpose of the present work is to use experiments that have been performed at Forschungszentrum Karlsruhe during about the last ten years for determining the most appropriate models and parameters for premixing calculations. This is done by recalculating experiments in two steps:

1. The results of a QUEOS experiment [2, 3] are used to fix the parameters concerning heat transfer. The QUEOS experiments are especially suited for this purpose as they have been performed with small hot solid spheres. Therefore the area of heat exchange is known. In addition, care has been taken to match the relevant conditions as close as possible. This concerns the initial temperature of the spheres which was at or beyond 2000 K, the size and number of the particles, and the typical mixing situation.

2. With the heat transfer parameters fixed in this way, a PREMIX experiment [4] is recalculated. These experiments have been performed with molten alumina (Al_2O_3) as a simulant of corium. Its initial temperature is 2600 K. With these experiments the models and parameters for jet and drop break-up are tested.

In any experiment performed to study the intensive thermal interaction between a very hot phase and cold water, the pressure history is the measurement that tells us most about what has been going on. This is because the pressure can be measured very well and depends critically on evaporation and condensation.

However, if the steam that is created can flow away freely, the pressure will depart only slightly from the environmental pressure and the pressure history will not be very conclusive. Therefore the above two experiments have been chosen on the basis of

a) an important and violent thermal interaction taking place, and
b) a clear pressure development being observed.

These conditions led to the choice of the above experiments that have been conducted with important masses of hot materials, with limited amounts of water present, and in closed vessels.

2. The QUEOS experiments[2, 3]

These experiments have been performed with solid spheres to provide data on heat transfer within a multiphase mixture with a known heat transfer surface area. The experiments where performed in a square vessel, 0.7 x 0.7 m, 1.38 m high, see Figure 1. The water depth was always 1.0 m.

The top of the vessel was closed except for the (gas tight) falling channel of the spheres in the center. Three of the walls were almost completely made of glass so that the mixing process could be filmed against a black background and, at a right angle to that direction, against an illuminated background.

Two venting pipes with different diameters were available and some experiments have been performed with both of them shut off, i.e. a closed vessel. Besides the high-speed movies of the mixing process, the main measurements where the temperatures of the spheres and the water, pressures in the vessel and in the vent tubes, steam flow rates, and, later on, the local void.

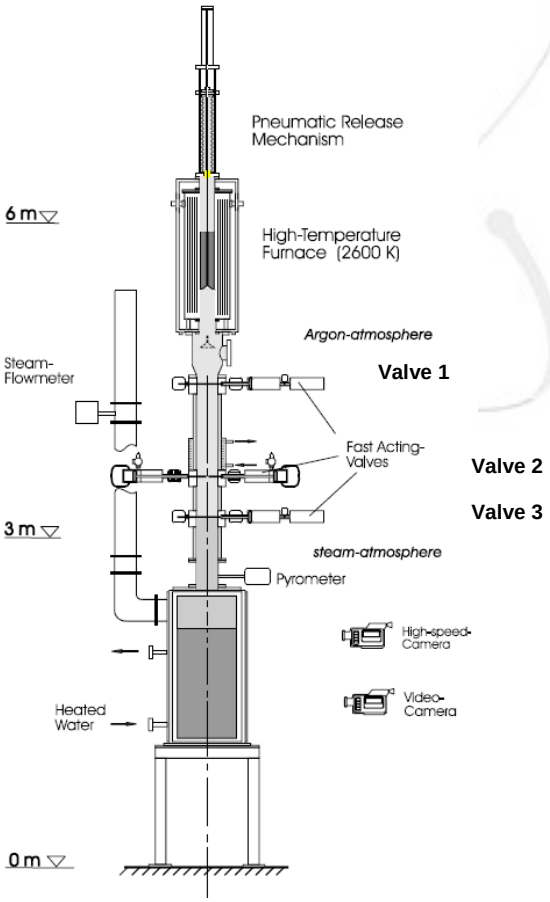

Figure 1: Scheme of the QUEOS facility

2.1 Experiment Q58

This experiment was performed with 10.84 kg (about 28,000) spheres made of ZrO_2 with a radius of about 5 mm and a temperature of about 2100 K. Figure 2 shows the propagation of the spheres through the water pool. The initial diameter of the sphere jet was 0.18 m. The water was slightly subcooled by 2.3 to 3.2 K.

Both venting lines were closed so that the vessel was closed except for a small pressure release valve that was used to keep the pressure at 1 bar while the hot spheres were resting on the sliding doors from which they were released into the test vessel (the water pool) after closing a gas tight valve between this location and the furnace and opening a similar valve between this location and the vessel.

The release valve had a diameter of 12 mm, a complicated internal geometry, and it was spring loaded to prevent inflow of gas. So it caused a very small leak flow. The leak flow was cut off at about 1.47 sec after release of the spheres (time 0.0) when the gas tight valve between the test vessel and the sliding doors was closed again.

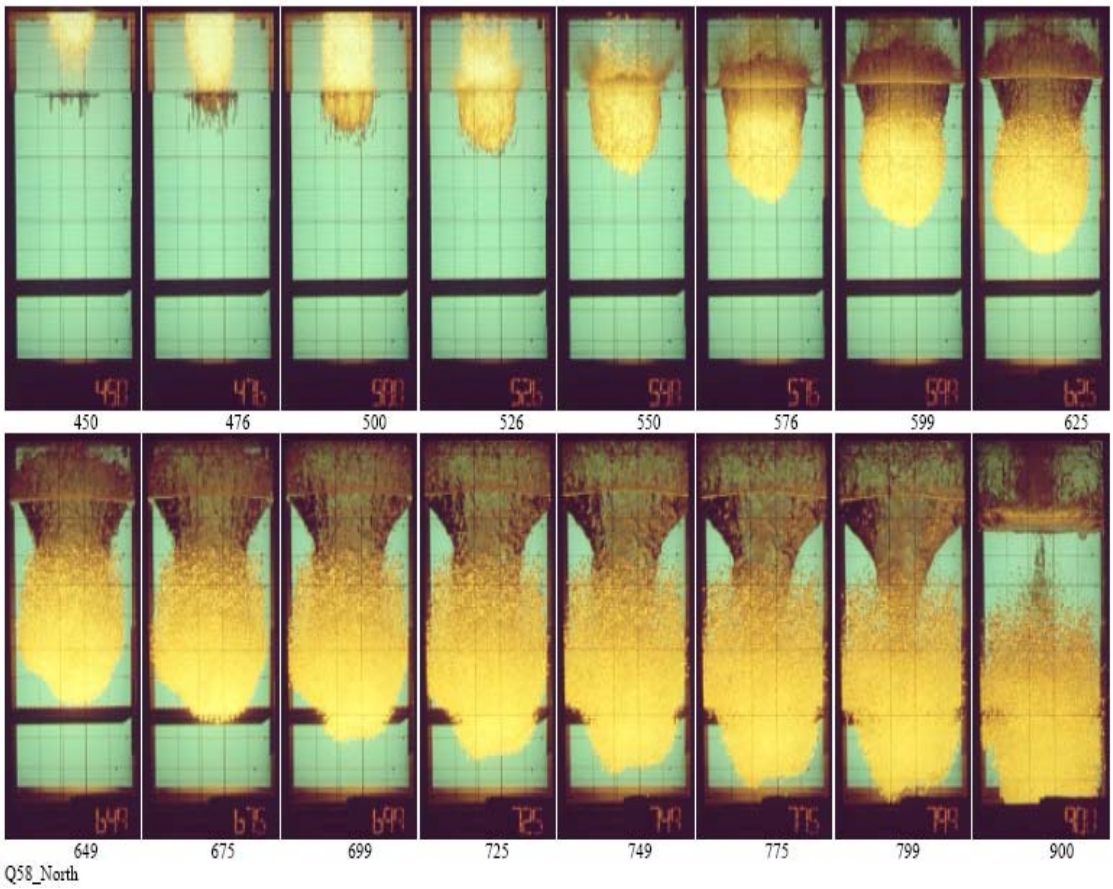

Figure 2: High-speed movie pictures of QUEOS experiment Q58. The numbers indicate the time in milliseconds.

Figure 3 shows a combination of some measured data. Obviously, the pyrometer (Maurer) reading is in Kelvin, not in centigrade. The scale on the left has no meaning.

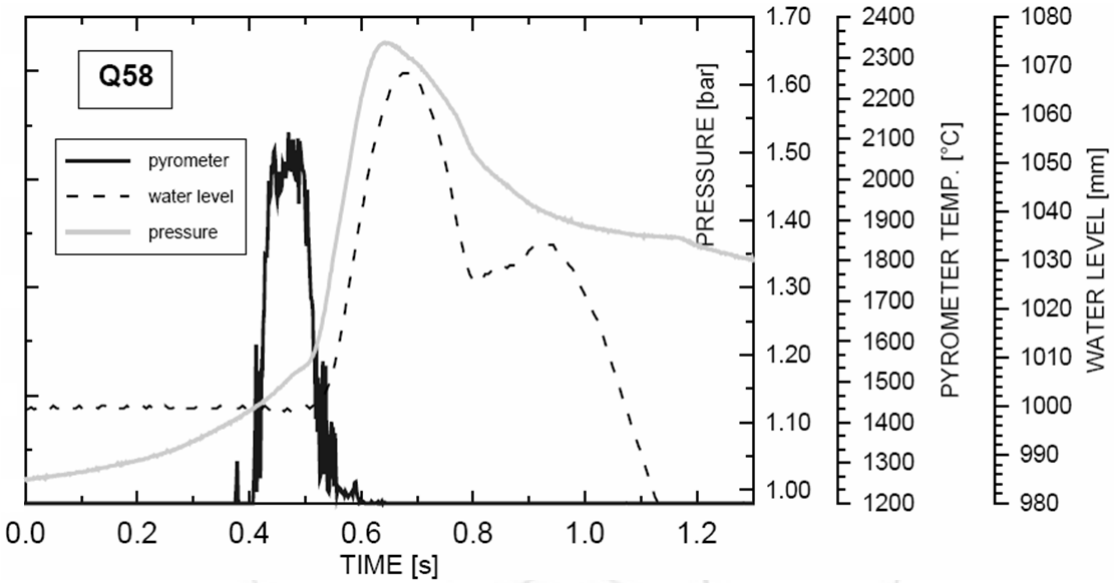

Figure 3: Compilation of measurements in experiment Q58 (from Ref. 3).

This experiment is characterized by a very steep pressure rise (about 1.1 MPa/sec) after contact of the spheres with the water and an about half as steep decay after going through a sharp peak at about 0.166 MPa. This peak occurred at 0.67 sec, i.e. 0.17 sec after contact between spheres and water. From about 1.5 sec on, the pressure remained almost constant at about 0.13 MPa.

Such behavior was observed in two tests performed with slightly subcooled water, while two similar tests with saturated water showed the expected (about exponential) pressure decay towards a much lower level (about 0.11 MPa). This behavior seemed to be difficult to understand in the beginning.

The explanation is that in all tests the water was heated to saturation and kept at that level for a long time to heat all structures in contact with the internal atmosphere to that level as well. (Some heating was done from outside also.)

In case of the tests with subcooling, the vessel then was opened and the water was allowed to cool to the desired level. During this period, some of the steam in the vessel condensed and was replaced by air. Later, during the test, this initially cooler air was heated and caused the elevated pressure plateau together with the also somewhat raised saturation pressure of the water.

The occurrence of an (almost) constant pressure indicates thermal equilibrium. This state was reached shortly after the leak path was closed off. Apparently the partial pressure of the air prevented further effective cooling of the hottest water in contact with the inner atmosphere (which defines the partial pressure of the steam) by evaporation.

Further cooling occurred by convective mixing with colder water and conduction only, so that the steam partial pressure decreased only very slowly after closure of the leak path. During this phase the spheres are still very hot and boiling occurs on them. But all vapor created thereby is condensing in the large amount of cold water above.

Of course, the thermal equilibrium discussed above isn't really global (inside the vessel). The spheres still have high temperatures and there are temperature differences within the water. But the steam created by the hot spheres on the bottom of the vessel condenses deep in overlying cold water without affecting the temperature of the water close to the surface of the pool.

A special feature of experiment Q58 (as of some more in that range of the experimental series) is the measurement of void. This was a time-resolved local measurement along two lines 60 mm apart in a plane 0.4 m above the bottom of the vessel. Thin wires forming the probes at their tips extended 30 mm on both sides of a support bar. This bar ran parallel to two of the vessel walls through the vessel center and they carried local resistance void probes every 20 mm.

For the purpose of comparison with calculated data, the original data have been integrated over a small time window and several of the void probes. The three innermost ones on both sides span an area of 60 x 60 mm. These are used to obtain the 'central' void. Similar arrangements about the locations ± 15 cm (along the support bar) give the data at radius 15 cm.

For timing, we also use the data of two pyrometers looking at the sphere jet at the level 1244 mm. It appears that the Maurer instrument has a larger viewing field (or is more sensitive) than the Keller instrument, because it registers spheres for a longer period. So, the Keller 'sees' spheres from 0.42 sec to 0.54 sec with some additional peaks up to 0.59 sec, while the Maurer registers a 'forerunner' just before 0.38 sec and a main stream from 0.40 to 0.60 sec with the signal quickly decaying after 0.52 sec. So, a 'length' of the jet of 0.12 sec seems to be a reasonable value and the passage starts at 0.041 ± 0.01 sec.

From the so measured length of the sphere jet, 55 ± 3 cm, an average volume fraction of the spheres within the jet of 0.13 has been derived. Nothing is known about the internal distribution of the spheres in the jet. Actually the above length is larger than can be calculated with free fall assumptions and also larger than observed with cold spheres. There is some not understood effect, leading to more spreading of the sphere jet in axial direction.

Additional information on timing can be obtained for the level of the void sensors, 0.400 m. The movies showing the motion of the particle cloud indicate that the level is reached at about 0.65 sec. The big void peak observed in the center of the vessel starts at 0.67 sec.

2.2 Recalculation of Q58

2.2.1 Setup and initial conditions

The experiment is simulated in the present work in cylindrical symmetry using 17 radial and 64 axial meshes (cells). The spheres are held initially in volume given by 3 radial times 3 axial cells. Figure 4 shows a plot of the mesh (from PPJET, a post-processing tool coming with MC3D) including the no-flow zones (in black), the initial pile of spheres (indicated by dots), and the water pool (in blue/light grey).

The scales in radial and axial directions are different in this figure. The radius of the pool is 0.4088 m, its height 1.0 m. The experiment is simulated from level zero (bottom plate) up to level 3.174 m, i.e. the uppermost gas-tight valve. The upper part of the tube in which the spheres had been falling to the sliding doors is increased in radius (while preserving the volume) in order to reduce the total height of the calculation region. The thin plate serves to guide the gas in such a way that all gas is involved in the flow towards the leak which is in the top center. (Such plates have zero thickness.)

The leak is modeled with its maximum possible size (12 mm diameter) by assigning a corresponding permeability (0.0225) to the mesh cell below the boundary at which the boundary condition was applied (the top center cell). Inflow of gas from outsides during the very initial phase of the sphere movement which caused a very slight pressure reduction in the space above was prevented by setting all volume fractions on (the outer side of) the boundary to zero.

In the initial state the spheres are lying on the sliding doors in dense sphere packing, i.e. with a volume fraction of 0.67. This requires to set the ‘solid pressure,’ a numerical artifact that shall prevent ‘overpacking’ (volume fraction > 1) of a field in a cell, to zero. It is no use in this simulation, anyway.

Except for converting the square vessel onto a circular pool with 0.4088 m radius and the change in geometry on top, the geometry corresponds exactly to the experiment. However, as variable geometries (permeabilities) are not available in MC3D, the opening of the sliding doors which releases the spheres within 50 msec could not be modeled. (Anyway the progressive opening of a slit across the bottom of the tube holding the spheres cannot be modeled closely in cylindrical symmetry.)

So, the bottom below the stack of spheres is just open at time zero. In this way, the full experiment is simulated, including the drop of the spheres towards the water surface. This process, of course, is affected by numerical diffusion. But MC3D uses a second order Van-Leer scheme so that the effect is somewhat reduced.

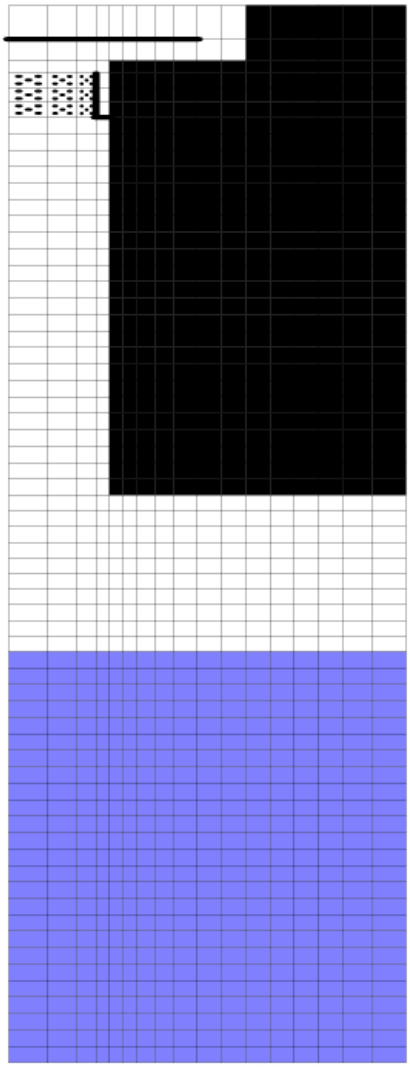

Figure 4: Calculation region for QUEOS simulation with meshing (thin black lines), no-flow zones (black areas), guide sheets (thick black lines), and the initial positions of water (blue/grey area) and spheres (black dots). The scales are different in the two directions.

The initial pressure in the gas room is 0.1016 MPa (barometer reading) and the hydrostatic pressure is added in the water. The initial temperatures are 2100 K in the spheres and the gas surrounding them as well as above them, 371.0 K in the water, and 370.1 K in the gas above the water. The temperature of the gas (argon) between the sliding doors (level 2.300 m) and the lower gas tight valve (level 1.925 m) was increased slightly because this gas was heated somewhat while the spheres were resting on the closed (but not gas tight) sliding doors.

The atmosphere above the water (up to the level 1.925 m) was assumed to contain 7 % (by volume) of air. As MC3D doesn't allow varying this fraction of

incondensable gas independently from the gas temperature, an additional volume of pure air was added (in place of some of the normal atmosphere) on the outside of the gas space to simulate the air that had entered the test vessel atmosphere during the cooling period. For this, a volume of 0.0195 m^3 and a temperature of 300 K were assumed.

The sphere radius was assumed to be 5.07 mm corresponding to the hot state. The cold diameter is 4.95 mm.

For this case, of course, the solid sphere option (BILLE) of MC3D was used with the available material ZIRCONE which assumes a density of 5900 kg/m^3.

2.2.2 Models and parameters

An important result that became immediately obvious was that the intense thermal interaction between the spheres and the water could not be reproduced with the standard (recommended) film boiling model in MC3D that is based on the Epstein-Hauser correlation and adapted to data from Liu and Theofanous. Similarly bad results were obtained with the classical Epstein-Hauser correlation and the correlations by Liu and Theofanous, as well as by Bromley.

Only the correlation by Dhir and Purohit gave reasonable results. To obtain the same sort of results with the Epstein-Hauser correlation at least initially, its heat transfer coefficients had to be multiplied by a factor of about five. This large factor highlights how strongly the heat exchange in a highly agitated multiphase mixture deviates from what is observed on single large spheres at rest or with small forced convection velocities.

The so obtained high heat transfer causing a high evaporation rate as well, had to be counterbalanced by a similarly strong increased condensation. This is more difficult to obtain in MC3D. The most effective way proved to be prescribing small diameters of the water droplets and, above all, the bubbles. Their sizes can be influenced by setting minimum and maximum values for the diameters and, to some extent, by the fragmentation models applied.

Unfortunately, the Meignen bubble fragmentation model (invoked by the option IOPT 76 2) which gave the best results for the rising flank of the pressure peak, gave unsatisfactory results later on so that it couldn't be used. However, varying the critical Weber number in the standard fragmentation model has a somewhat uncertain effect on the bubble size as it mostly jumps to and fro between the maximum and minimum values that are prescribed.

Values in between are mostly observed when the bubble radius is newly initiated after leaving the drop flow regime and entering the transition region. But how this

value is determined is neither known nor obvious and, thus, eludes control. In this area, better parameter choices than found in this work could possibly be found.

The properties of the film boiling models available have been studied in a certain situation resembling the base case described below. The following table shows the results concerning the maximum heat transfer rates. In that, 'Conduction' means conduction through the film (MC3D output variable FLFBS) and 'Radiation' stands for radiation to the liquid (MC3D output variable RDRLS). These two are by far the most important heat transfer modes.

Table I: Comparison of film boiling correlations

Film boiling model	**Conduction**	**Radiation**
EPSTEIN-HAUSER modified	1.7 E 06	1.1 E 06
EPSTEIN-HAUSER modified, with factor 1.7	3.0 E 06	1.1 E 06
EPSTEIN-HAUSER modified, with factor 2.0	3.45 E 06	1.1 E 06
EPSTEIN-HAUSER modified, with factor 4.0	6.8 E 06	1.1 E 06
Classical EPSTEIN-HAUSER	3.5 E 06	1.1 E 06
Liu-Theofanous	1.93 E 06	1.2 E 06
Dhir-Purohit	8.4 E 06	0.8 E 06
Dhir-Purohit with increased condensation	7.3 E 06	0.65 E 06
Bromley	1.93 E 06	1.2 E 06

The initial pressure rise, prior to the spheres contacting the water, is solely due to heat transfer from the spheres to the gas. Without assuming increased gas temperatures above the lower valve (level 1.925 m), this pressure rise was too high. But assuming a linear temperature gradient from 625 K (at the top) down to 425 K (at the bottom) between the valves, gave good agreement with the experiment. So, there was no reason to modify the heat transfer coefficient between spheres and gas.

Unfortunately things become much more complicated when the spheres have entered the water and the pressure development actually seen is the result of the balance between a large evaporation rate and a similarly large condensation rate, where, at first, evaporation prevails and, later on, condensation. The first spheres touch the bottom of the vessel (in the simulation) after about 1.1 sec. At this time the peak values of pressure and void have been passed and the pressure has already decreased considerably.

So, the main pressure peak and the first void peaks are not influenced by the settling of spheres on the bottom. It is important to note this because the special conditions of heat transfer between spheres 'lying on the bottom' and water are insufficiently modeled in MC3D as in most other codes. Therefore deviations of the simulation from the experiment at times well after 1 sec may be due to this shortcoming and cannot be interpreted as deficiency of other models in the code.

The first phase of the experiment, the fall of the spheres towards the water surface, is well described by the code. In free fall, the spheres would arrive at the water surface at 0.515 sec with a velocity of 5.05 m/sec. When modeled without drag between spheres and gas and when a local sphere velocity is fully developed (when the volume fraction of spheres in the donor cell has reached a certain level), the velocity equals exactly free fall velocity.

Still the spheres arrive at the water surface about 0.03 sec (6 %) too early. This is the consequence of the stretching of the sphere cloud in the direction of motion by numerical diffusion. The effect amounts to only about 6 mm at the front, but is more important at the trailing edge.

However, the entrance of the spheres at the trailing edge of the jet into the water pool is strongly inhibited by the steam produced by the spheres that are already within the pool. So, the distortion by numerical diffusion may not be too important. With full (default) drag between gas and spheres in action, the falling time is increased by about 0.02 sec (4 %) and the spheres arrive with a velocity of 4.7 m/sec.

Of course, the results of the thermal interaction that follows depend to some extent on the concentration of the spheres (their volume fraction) when entering the water. This concentration has an important influence on the mixing ratio between hot material and water. In the parameter range realized in the present calculations, a smaller sphere concentration leads to a higher maximum pressure.

Calculated with standard parameters, the cloud length was too small in the calculations (in spite of numerical diffusion), as measured by the time it needs to fall by the level of the pyrometer. It was found that the strongest influence on this variable was due to a model parameter that has no direct physical meaning, i.e. the ‘film thickness’ which is used in the calculation of the gas that is transported with drops (or spheres at that).

It is designated as ‘film thickness in film boiling’ but, apparently, is active with spheres in single-phase gas as well. Choosing this parameter as 0.3 mm (somewhat outsides the range of 10^{-6} to 10^{-4} recommended in a recent draft of a support guide for MC3D), a jet length of slightly over 0.1 sec was obtained. Much larger values of this parameter (0.5 mm and beyond) cannot be used because they cause unphysical distortions of the sphere jet.

While the spheres arrive at the water surface slightly too early, they arrive at the level 0.4 m, where the void sensors are installed, at 0.743 sec, about 0.1 sec too late. This means that the spheres are progressing through the water too slowly. This can be avoided by reducing the drag between liquid water and spheres by a factor 6…10.

But this, at the same time, has an influence on the radial distribution of the spheres so that, with much reduced drag, very few spheres pass at the radius 15 cm and consequently the void observed there is also much reduced in contradiction with the experimental observations. Therefore the drag was not modified.

2.2.3 The base case (best fit)

The following figures show the results of the calculation (case 146) that is judged to give overall the best results. The main criteria are the timing and the peak value of the main peak. These are shown in Figure 5. The agreement in the initial phase was obtained by setting the initial value and fitting the pressure at 0.3 sec (via the preheating of the gas above the lowermost valve).

The rest of the pressure development is a result of the heat transfer (to the vapor and to the water) that cannot be influenced in detail. The peak pressure was fitted by adjusting the minimum bubble radius. It is obvious that the steep pressure rise of the experiment could not be reproduced fully. Less drag of the spheres in the water and less condensation gave a better approximation but had disadvantages in other aspects.

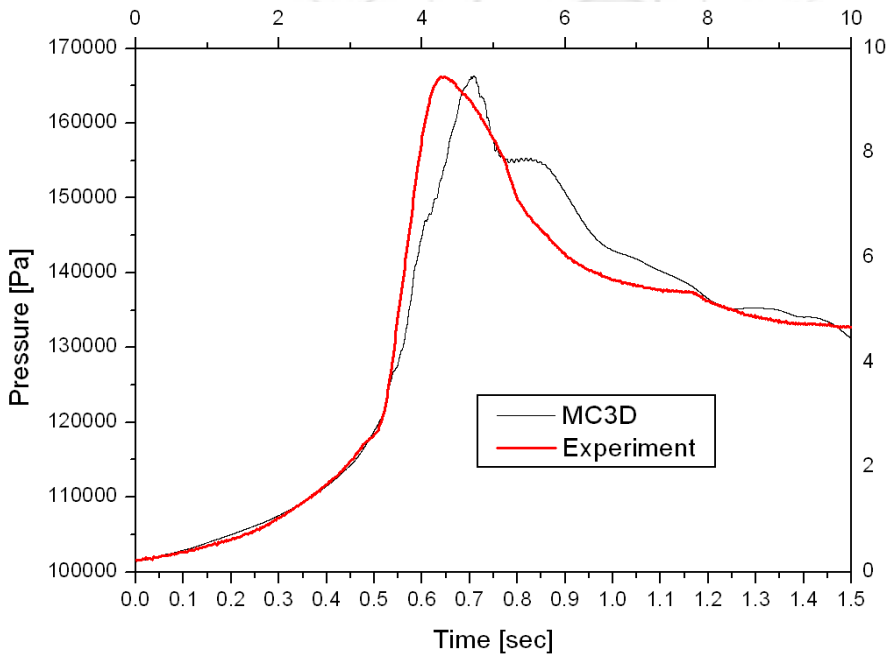

Figure 5: Comparison of experimental and calculated pressure development in the gas space of the test vessel in the initial phase.

Figure 6 shows the pressure histories over a longer period. The pressure level after 1.5 sec was roughly adjusted with the help of the amount of non-condensable gas in the atmosphere. However, the vivid pressure variations in the calculated results show that thermal equilibrium is not as well established in the calculation as in the experiment. This may, however, be a consequence of too strong boiling from the spheres lying on the bottom of the facility.

Here one might mention that, in these calculations, the option IOPT 81 has been used to choose the application of the Bromley correlation for film boiling in the lowermost row of cells (k=1). The fact that this possibility has been included in MC3D suggests that the Bromley correlation is especially suited to describe the reduced heat transfer expected for particles resting on the bottom.

However, in a test of the film boiling correlations (see discussion above in 2.2.2), the Bromley correlation was not found to give especially low heat transfer rates. The modified Epstein-Hauser correlation gave about 10 % less heat transfer and the Liu-Theofanous correlation gave the same result as that of Bromley.

But the Bromley correlation is the only one that can be chosen to be applied in special regions instead of the main correlation and its heat transfer rates are only about 23 % of that of the Dhir-Purohit correlation. An attempt to modify MC3D as to use a much reduced heat transfer in this special application of the Bromley correlation (by adding a single statement reducing the heat transfer), completely marred the calculation.

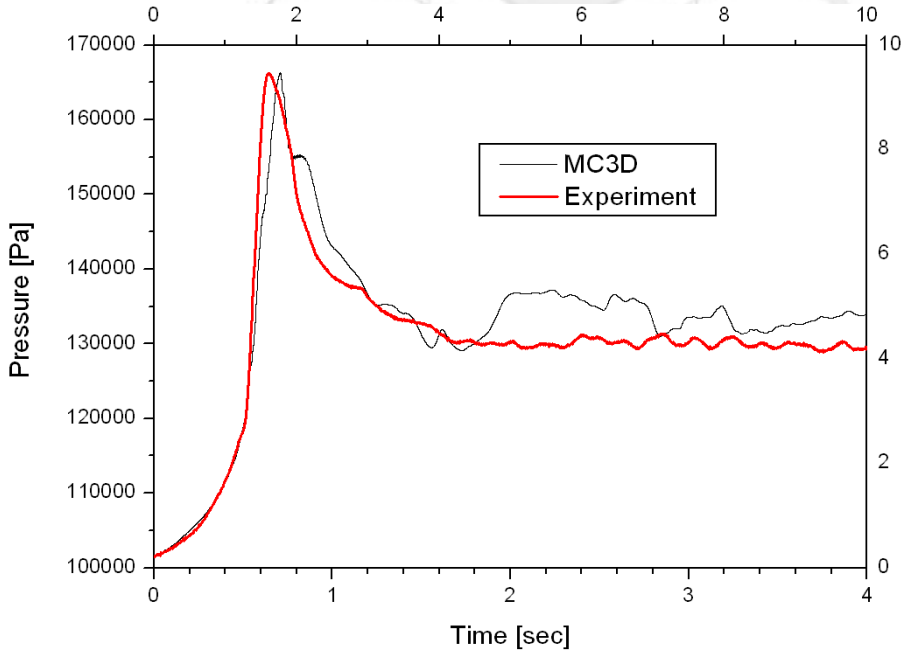

Figure 6: Comparison of experimental and calculated pressure development in the gas space of the test vessel.

The second criterion for choosing the base case calculation was the result concerning the void. The measured void is characterized by a high void at the center and a much lower value at radius 15 cm, with most of it appearing somewhat later. Although the calculated voids don't really match the measured ones and were quite sensitive to parameter changes, these two main properties could be found in several simulations.

Figure 7 compares the void measured and calculated at the central position (up to radius 3 cm). Here the gas volume fraction is somewhat sketchy denoted as void because the sphere volume fraction in the corresponding volume is always small.

It is obvious that the calculated void comes too late, is not large enough but lasts much too long. The delay is partly due to the belated arrival of the spheres at the level of the void sensors (0.400 m) which occurs at 0.71 sec instead of 0.65 sec. An additional delay occurs because the void initially grows only slowly (as the sphere void fraction grows, see below). A similar thing might have occurred in the

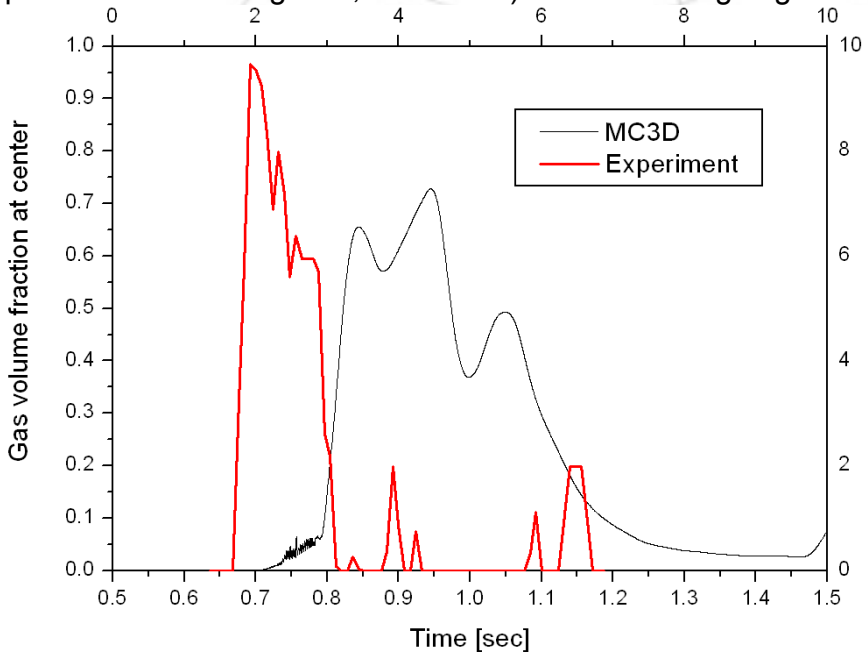

Figure 7: Comparison of experimental and calculated void histories

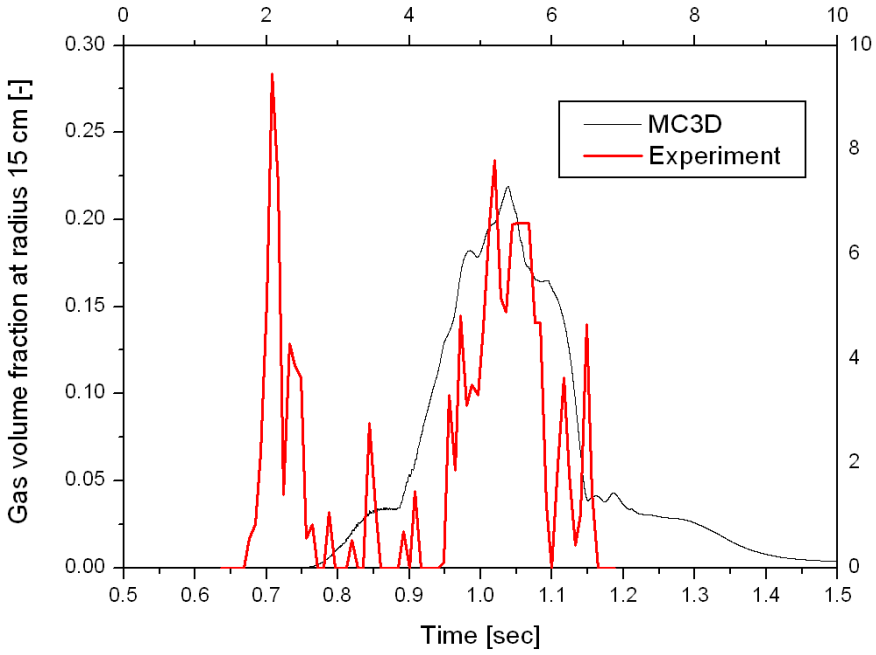

Figure 8: Comparison of experimental and calculated void histories at 15 cm radius. Mind the different scale on the ordinate.

experiment and just not have been registered because being too low (the first non-zero data point is about 30 %). But if so, this period could at most have taken 0.02 sec and not 0.08 sec as in the calculation.

In a calculation with the drag between liquid water and spheres reduced to 15 %, the spheres (correctly) reached the measurement level at 0.65 sec and the void started to grow (even earlier!) at 0.64 sec reaching a maximum of 90 %, but spheres and void were practically absent at 15 cm radius. Therefore the default drag was used. (At about 1.5 sec there follows a second peak about 20 % high that has no counterpart in the experiment.)

Figure 8 compares the void measured and calculated at 15 cm radius. In contrast with the experiment, the void starts to grow 0.05 sec later than at the center. So, the first peak is completely missed and the good temporal agreement with the second peak might be purely fortuitous.

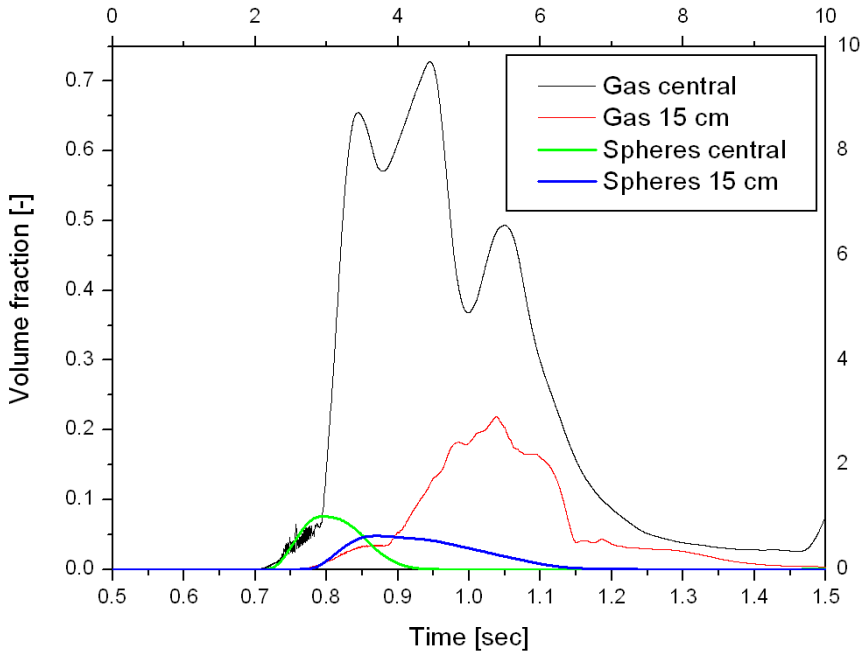

Figure 9: Correlation of gas and sphere volume fractions at the level of the void measurements (0.400 m).

Something that cannot be observed in the experiment is the correlation between the volume fraction of the spheres and that of the gas.

Figure 9 shows them for both locations monitored. In both cases the void starts slightly before the spheres arrive and the gas volume fraction remains similar to that of the spheres initially. That seems to be reasonable as close-ups of the sphere cloud obtained in some experiments show that, in the front, every sphere is surrounded by an individual vapor film that may have a similar volume. Trailing behind the spheres are vapor channels (irregular tubes) that later on may merge into volumes in which the gas is the continuous phase.

Consistent with this observation, the gas volume fraction starts to outsize that of the spheres somewhat later. In the calculation this happens roughly when the sphere volume fraction has reached or just exceeded its maximum. So, this calculation indicates that roughly half of the hot spheres are traveling in an environment in which the gas volume fraction is equally small as the sphere volume fraction and only the other half is surrounded by a higher gas volume fraction – such that melt drops in such an environment could possibly not participate effectively in a steam explosion.

This means that the void, besides its cushioning effect, is not the primary quantity of concern in steam explosion calculations. Rather the explosion potential of a

premixture should be judged on the basis of the fraction of coarse fragments that are surrounded by continuous water.

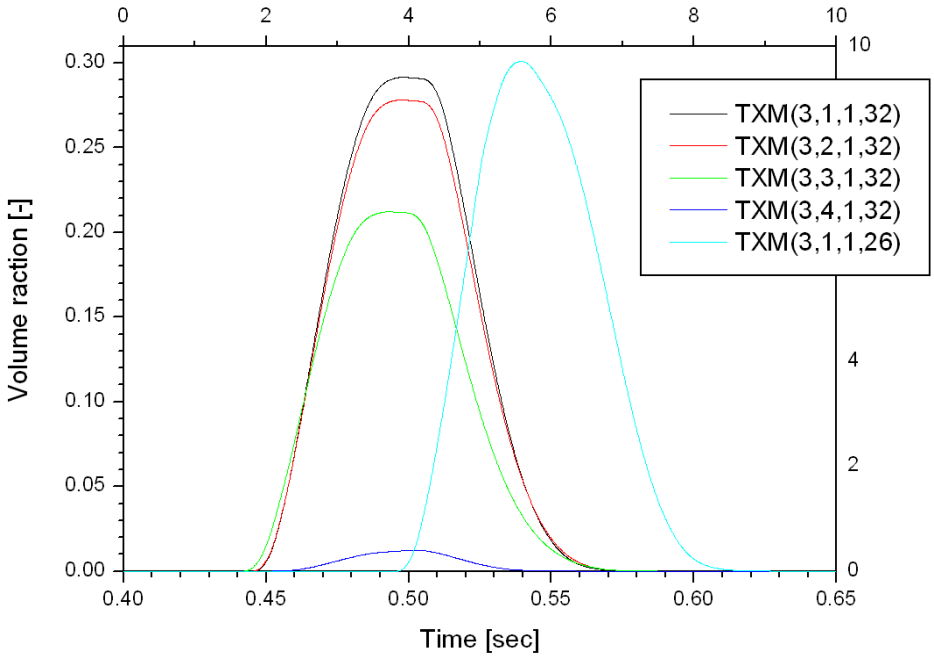

Figure 10: Volume fraction of the spheres (l=3) in cells at two axial levels (k=32, i.e. the level of the pyrometers and k=26, i.e. the first cell above the water surface). At the upper position, the four innermost cells are shown (i=1,…4). The legend is TXM(l,i,j,k). The azimuthal coordinate (j) is always 1 because cylindrical geometry has been used.

Figure 10 shows some time dependent volume fractions of the spheres [TXM(3,…)] in individual cells at two levels above the water. The indices shown are (l,i,j,k). At k=32 the pyrometer is located and the four innermost cells are plotted. This shows that, at this level, the sphere jet has slightly widened radially and that the spheres have fallen a little faster in the third ring (radial mesh), probably because of less drag between gas and spheres.

The slight radial extension may be consistent with what is seen in Figure 2, but the radial profile at the leading edge is not. It cannot be as the finite opening time of the sliding doors releasing the spheres is here not modeled. At the level k=26, just above the water surface, the cloud has become shorter and the maximum sphere concentration has slightly increased. This is again a consequence of drag between gas and spheres.

Figure 11 illustrates the enormous importance of film boiling heat transfer (conduction: MC3D output variable FLFBS and radiation: MC3D output variable RDRLS) in conditions as simulated in the QUEOS experiments. It is by far the

largest heat flux from the spheres to the environment. (The black and green curves of figures like this have been the source of data in Table I.)

Typically about one quarter of the heat delivered to the gas/water interface is lost (does not generate vapor) by conduction into the bulk water (MC3D output variable FINTL). Compared to that, heat losses from the steam to bulk water (MC3D output variable FVINT) are negligible (a factor 15 smaller).

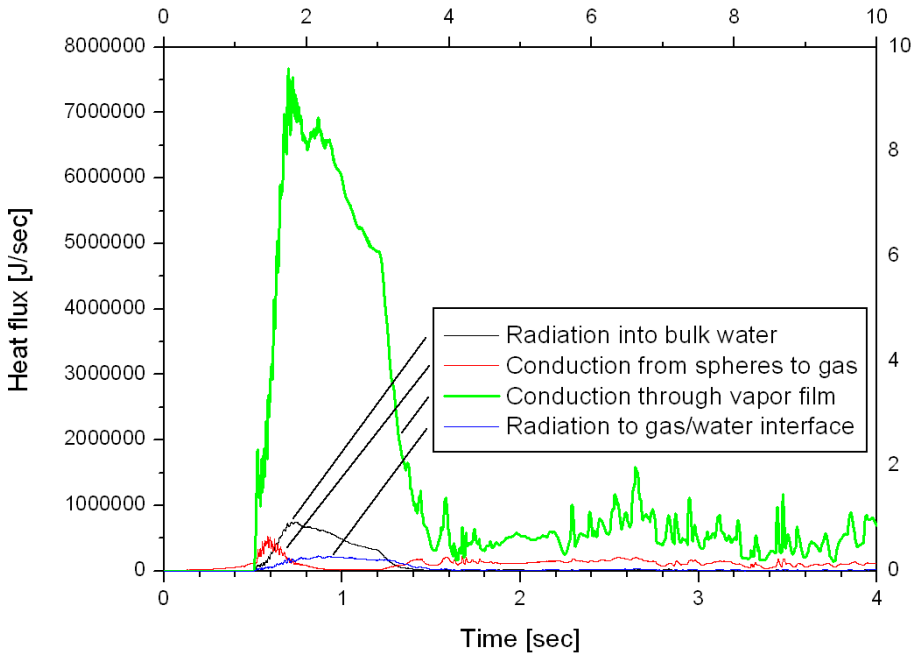

Figure 11: Comparison of the most important heat fluxes, integrated over the whole calculation domain.

As already indicated, the overall evaporation and condensation rates are of similar size and only the much smaller difference between them is creating pressure. So, in Figure 12, the (negative) total condensation rate (MC3D output variable GC) has been added to the total evaporation rate (MC3D output variable GE) to show the net evaporation rate.

Its maximum is smaller by about a factor three and occurs during the very first part of the rise time of the two individual total rates. Apparently the outbreak of condensation shortly after 0.7 sec is responsible of the steep pressure decrease at this time (cf. Figure 5).

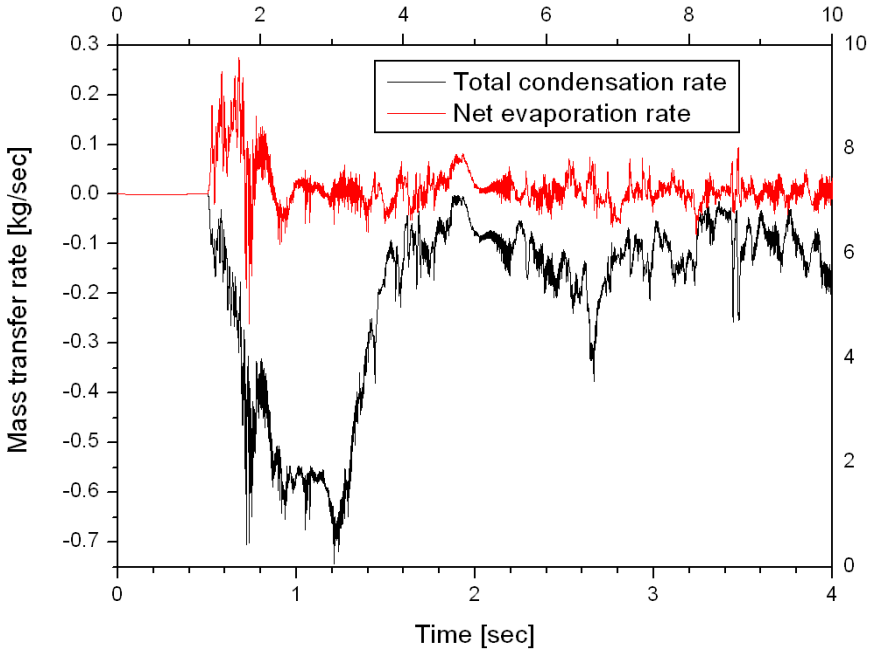

Figure 12: Mass transfer rates, integrated over the whole calculation domain.

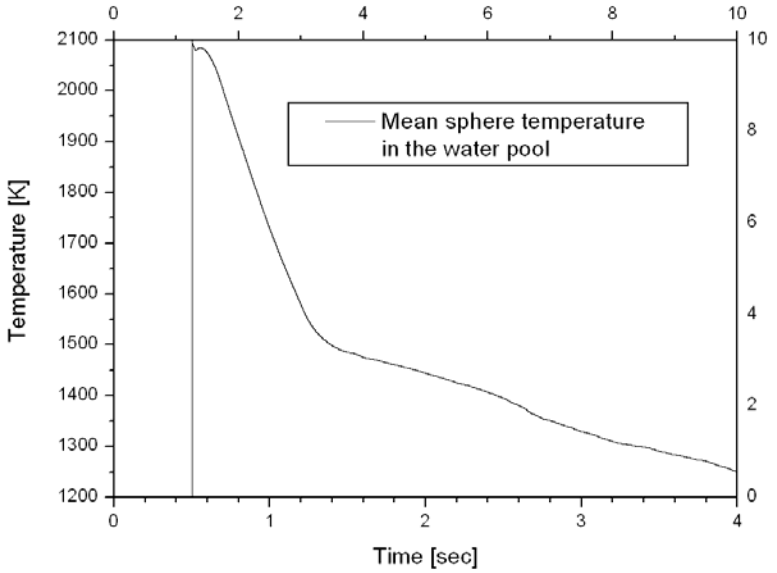

Figure 13: Mean sphere temperature in the water pool.

The above discussed strong heat transfer from the spheres leads to a fast cooling (quenching) of them, as shown in Figure 13. As can be seen, the quenching is especially strong between about 0.55 sec, when most of the spheres have entered the pool and about 1.4 sec, when all spheres have settled on the bottom. From then on, they are cooling at a much reduced but still considerable rate.

2.2.4 Variations of the base case

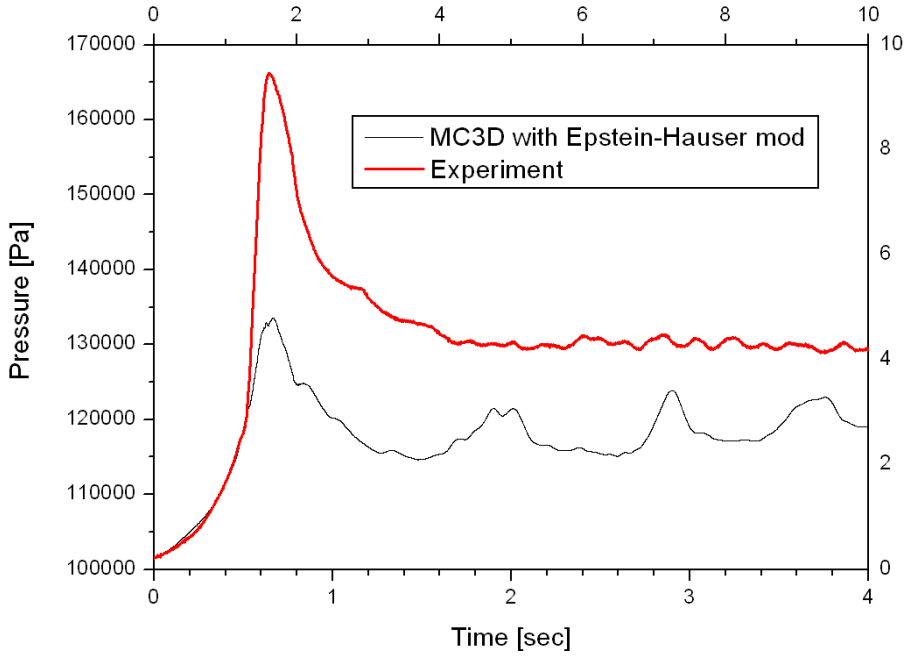

Figure 14: Comparison of experimental and calculated pressure development in the gas space of the test vessel when using the Epstein-Hauser modified film boiling model. All other parameters are identical to the base case.

To demonstrate the eminent significance of the film boiling model, the base case is repeated with just replacing the Dhir-Purohit model by (the default) Epstein-Hauser modified (case 148). The resulting pressure history is shown in Figure 14. Both, the pressure peak and the roughly constant pressure level afterwards are much reduced.

The base case has been calculated with the maximum possible leak flow, i.e. a free opening with 12 mm diameter (until closure at 1.47 sec). It was found that reducing the flow area to 60 % had practically no influence (case 83). But in order to demonstrate the possible influence of this leakage flow, the calculation was repeated with the leak closed (case 149).

The result concerning the pressure is compared in Figure 15 to the base case. The changes are quite understandable. The relatively strong influence of the closed leak on the long-term pressure comes from the fact that mostly non-condensable gas is lost through the leak: 13.1 g of air, i.e. 26 % of the initial 50 g, while 7.3 g of vapor are escaping. Practical remark: This calculation has taken only 35 % of the

calculation time of the base case. In the base case calculation, the Courant-Friedrich-Levy condition at the leak has much reduced the time step size.

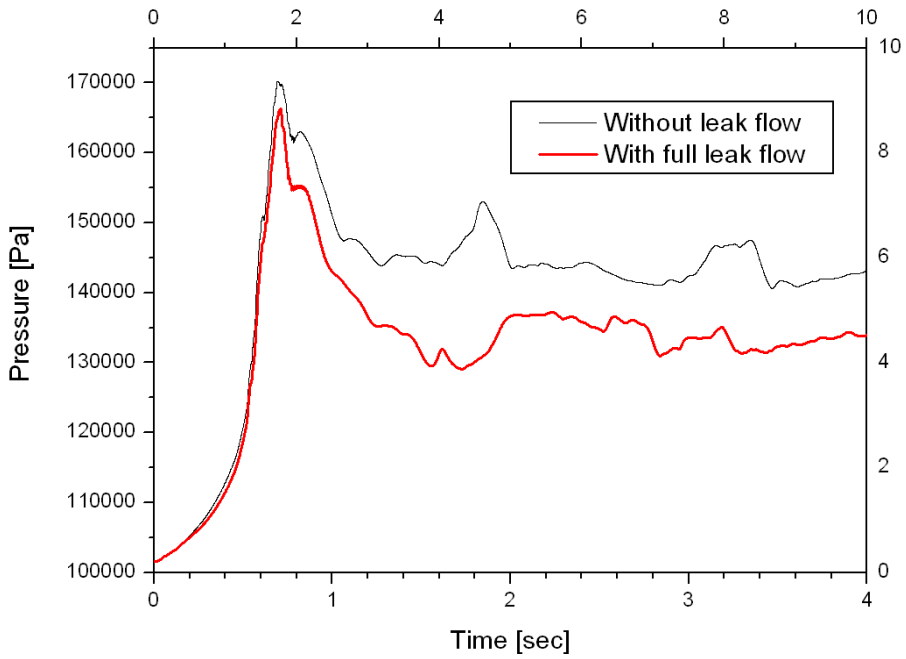

Figure 15: Comparison of pressure histories obtained with fully open and fully closed leak (pressure release valve).

2.2.5 Overview and discussion of models and parameters

The following is a list of the models and parameters used in the calculation that best resembles the experimental results. Except for the film boiling correlation and perhaps the somewhat strange 'film thickness,' none of these choices is out of the way (far from the recommended values).

Actually, there is no physical reason to limit the bubble size to such a large diameter. But pressure oscillations in the water and correspondingly the calculation time increase considerably if values below 1 mm are chosen. Also, both, the bubble and the drop diameters are not really adjustment factors.

The only reason to limit them (in either direction) should be numerical requirements (the stability of the calculation). But due to the lack of other possibilities, they are used here to adjust the overall condensation rate. As demonstrated by the distorted shape of the pressure peak (Figure 3), this is not a really good way to do it.

Table II: Models and parameters used

Heat transfer (HT):	
Film boiling mode	Dhir-Purohit
Multiplier for film boiling heat transfer	EPS_HAUS = 1.0
Bubble fragmentation	Default Weber number approach
Critical Weber number for bubbles	24.
Maximum bubble size	5 mm
Minimum bubble size	1.6 mm
Water drop fragmentation	Default Weber number approach
Critical Weber number for drops	12. (default)
Maximum water drop size	5 mm
Minimum water drop size	0.5 mm (default)
Bromley correlation for HT in the lowermost row of cells:	IOPT 81 1
Diverse parameters:	
'Film thickness'	0.3 mm: ROPT 85 .0003

The main disadvantage of using (essentially) the minimum bubble size to adjust the condensation is its rather haphazard (may be even inconsistent) local variation. This can be demonstrated with the reaction of the bubble diameter in the calculation cell from which the central void has been taken to a relatively small parameter change.

Figure 15 shows the variation of water drop and bubble diameters during the period enclosing the large void peak. Here the minimum bubble diameter is set to 1.1 mm. Figure 16 shows the same for a minimum bubble diameter of 1.6 mm.

In Figure 16 things look quite simple: When the spheres (and thus gas volume fractions beyond the minimum value) reach the cell, the bubble diameter quickly drops to the allowed minimum. (In this time, the diameter of the non-existing water drops is assumed equal to that of the bubbles. The same applies from 1.06 sec on.)

When the transition region (bubble and drop flow regimes combined) is reached (void > 0.3), the drop diameter jumps to its allowed maximum value while the bubble diameter starts to grow linearly.

When the transition region is left (void < 0.3), the bubble diameter starts to decrease linearly. It cannot be seen that this development had anything to do with the local conditions concerning the relative velocity between bubbles and water which should control the bubble size when the Weber number approach is used.

With the minimum bubble diameter increased by just about 50 %, things look completely different, see Figure 17: This time, the pure droplet regime (void > 0.7)

is reached at about 0.93 sec (as a logical consequence of reduced condensation) and the diameter of the no longer existing bubbles jumps to the drop diameter. When, shortly later, the flow regime returns to the transition region, the bubble diameter does not return to its previous (hopefully somehow rational) value but quickly drops to a value that varies from calculation to calculation in a way that doesn't suggest any system.

It then increases and decreases linearly, similar to the way it had done it in the previous case, but at a completely different level. After that, from about 1.4 sec on, follows a period in which the bubble diameter varies in a way that might be controlled by velocity conditions, until it stays fixed at the minimum value again.

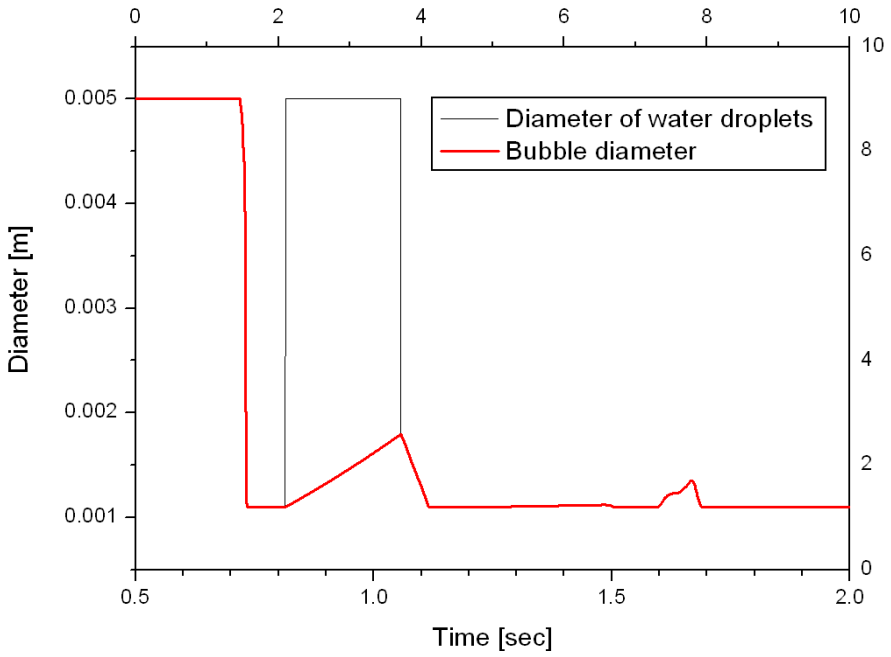

Figure 16: Diameters of water drops and bubbles in the cell from which the central void is taken. Minimum bubble diameter: 1.10 mm.

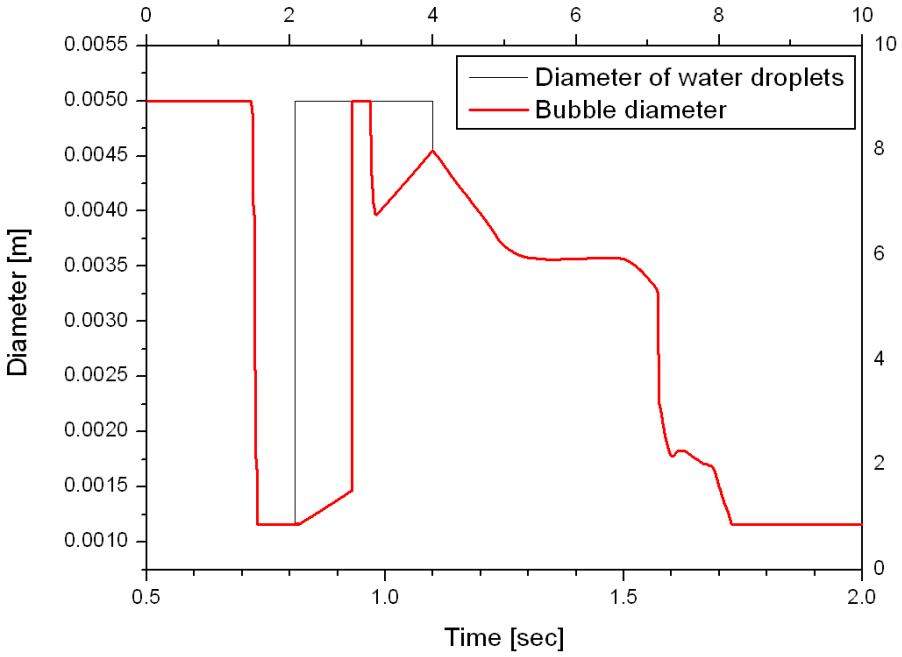

Figure 17: Diameters of water drops and bubbles in the cell from which the central void is taken. Minimum bubble diameter: 1.16 mm.

3. The PREMIX experiments

3.1 General

The PREMIX experiments are studying the full physics of premixing in that they really are observing the mixing of a liquid melt with water. In these experiments, corium is simulated by molten alumina (Al_2O_3) at a temperature of 2600 K. This is an oxidic melt which, with respect to volume and energy content, corresponds to about three times as much corium (in weight). The melt is produced by a thermite reaction and the liquid iron produced at the same time is separated from the oxide so that essentially the oxide is used in the experiment.

The test vessel is a high cylinder of 684 mm diameter with flat faces in front and back that are made of glass panes. The melt generator is housed in a cylinder with a radius of 0.200 m within the upper part of the test vessel, leaving an annular space to which the vent lines are connected.

The water is about 2 m deep but a debris catcher is installed1.33 m below the water surface. In most tests, the vessel has been open to the surrounding via vent lines but a few tests have been performed with these vent lines closed. Some of the tests, with or without closed vent lines, have been performed at elevated initial pressure (0.22 or 0.5 MPa). The melt mass and the diameter of the melt nozzle have been varied as well.

In the normal test procedure the thermite is ignited with electrical fuses and after completion of the reaction in the main volume of the melt generator, some time is allowed for the separation of oxide and iron (by gravity) and the iron melting its way into a previously evacuated retention chamber.

During this period the melt generator is vented and the chemical reaction proceeds through the upper part of the release tube until it reaches a steel foil that has sealed the melt generator in downward direction. When this foil is molten through by the hot melt, melt release starts. Shortly after that, the melt generator is closed and the gas above the melt is pressurized to a prescribed driving pressure. This normally leads to a fast melt release with corresponding strong break-up of the melt after melt-water contact.

Because the time of melt release was not controlled actively in these experiments, melt release occurred at different times after the time at which the experiment had been started. So, in order to make the experiments comparable to each other, time zero always was defined as the time of melt-water contact.

3.2 The experiment PM18

For the present purpose, experiment PM18 has been selected because it has been performed with a closed vessel so that a clear pressure increase occurs after melt-water contact. The experiment was performed with about 26 K subcooling at an initial pressure of 0.22 MPa. The melt generator provided about 15 kg of oxidic melt and the release tube had a diameter of 48 mm.

In order to increase the comparability with FARO tests, an attempt was made to simulate gravity release. To this end, a control system was used that increased the driving pressure above the melt when the pressure in the test vessel had come to within 0.02 MPa of the driving pressure. Actually, pressurization of the gas space above the melt started at 0.0595 sec.

In addition, the driving pressure was influenced by heat transfer from the hot surrounding to the gas (pressure increases) and by the release of melt (pressure decreases). This resulted in the pressure histories shown in Figure 18. Please note that the pressure in the interaction vessel shown (PKir15, red curve) is from a position deep in the water pool.

Another figure in the report shows that the pressure in the gas space is 0.0125 MPa lower. But the red curve, apparently, has been shifted in the figure to agree with the pressure inside the melt generator initially.

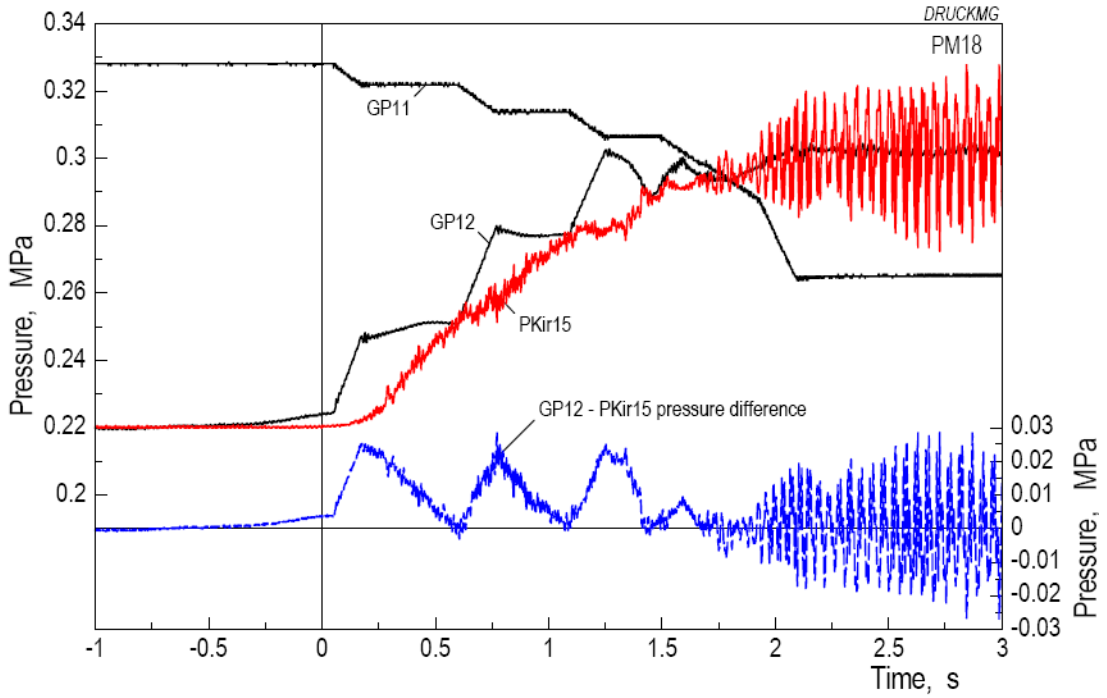

Figure18: Pressures controlling the melt release in PM18 (from Ref. 4)

From the pressure curves it can be inferred that a first blow-through from the melt generator into the test vessel occurred at 1.40 sec and the pressure in the melt generator dropped to that of the test vessel. As a consequence, gas was injected again into the melt generator and caused a short-lived overpressure.

Apparently the melt release tube had been blocked by melt again. But from 1.65 sec on the pressures are the same in melt generator and test vessel. From then on, only small amounts of melt may have dropped into the test vessel under the action of gravity. In total, 14.6 kg of melt have been released. So, the average melt release rate was about 10 kg/sec.

The water pool extended up to -0.05 m, giving a water depth of 1.33 m above the debris catcher. As the melt release nozzle was at 0.173 m, its distance from the water surface was 0.223 m.

3.3 Recalculation of PM18

3.3.1 Setup and initial conditions

Here again, the complete experiment is simulated including the melt release. Similar to Q58, it is simulated in cylindrical symmetry using 15 radial and 58 axial meshes (cells).

Figure 19 shows a plot of the mesh (again from PPJET) including the no-flow zones (in black), the initial location of the melt (red/dark grey), and the water pool (in blue/light grey). The scales in radial and axial directions are different in this figure. The radius of the (here) cylindrical vessel is assumed as 0.337 m.

The experiment is simulated from level -2.03 m (bottom plate) up to level 1.955 m, i.e. the top of the annular space around the melt generator. The debris catcher is simulated by thin plates. (Such plates have zero thickness.) Actually the debris catcher is not flat but curved, but that shouldn't play much of a role.

From the experimental data it has been inferred that melt release started at -0.32 sec. So, the times given for the experiment have to be increased by 0.32 sec when comparing with the calculation.

The melt mass assumed in the melt generator is about 16.3 kg, so that about 15 kg will be released (some melt remaining on the steps within the melt generator).

The geometrical conditions of water pool, debris catcher and melt nozzle are closely reproduced. However, it turned out that melt release was much too fast when the designed diameter of the melt release tube was used. So, a diameter of 36 or even 34 mm (instead of 48 mm) is used.

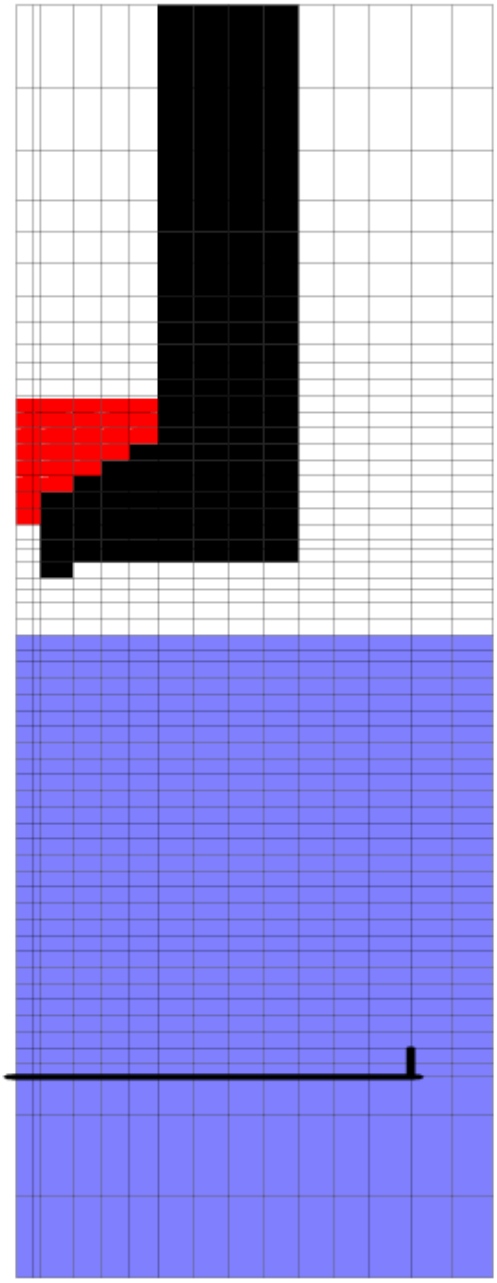

Figure 19: Calculation region for PREMIX simulation with meshing (thin black lines), no-flow zones (black areas), debris catcher (thick black lines), and the initial positions of water (blue/light grey area) and melt (red/dark grey area). The scales are different in the two directions.

This serves to simulate pressure losses at the tube entrance and within it, as well as a possible layer of frozen alumina (crust) inside the tube and, perhaps, a not complete melting of the steel foil that initially closed the melt generator downwards. (Such incomplete melting has been observed later in other experiments.)

The initial pressures in the melt generator and in the test vessel are assumed to be 0.220 MPa.

Initially it has been tried to simulate the pressure in the melt generator by simulating the gas addition to it. However, the attempt failed and so it was decided to simulate the pressure as measured in the melt generator directly, via a variable boundary condition.

As melt release is largely controlled by gravity and inertia, not all details of the pressure history have been reproduced in this way. In the figures that will follow, these rough data represent the experimental result. Unfortunately, pressure data are not available for plotting. The calculated pressure in the gas space should approach the knees at which the prescribed pressure in the melt generator starts to rise quickly, but should stay slightly below at all times prior to 1.77 sec (time in the calculation).

Of course, this type of boundary condition tends to make the result concerning the pressure in the interaction vessel look better: If the pressure remains too low, more melt is released which should increase the pressure, and vice versa.

A basic difference between the real situation in the melt generator and the one created by the boundary condition in the calculations is the infinite availability of gas in the latter which gains importance after a blow-through. To prevent that, the activity of the boundary condition is reduced to zero at time 1.572 sec by reducing the volume fraction of non-condensable gas in front of the boundary to zero.

This reduces the sum of the volume fractions at the boundary to zero. While this trick seems to be tolerated by the code, has the desired effect and doesn't cause immediate numerical problems, it might have contributed to numerical difficulties that often occurred some millisecond later. (But in all calculations that went that far, blow-through occurred earlier, ending the valid simulation anyway.)

3.3.2 Models and parameters

The calculations have been performed essentially with the parameters given in the table concerning the recalculation of Q58, except for the minimum bubble diameter (which was mostly 1 mm). Deviations from this will be mentioned explicitly. All calculations have been performed with the suggested (standard) options

- IALOPT 4 1 ('suivi de l'interface du jet' ≈ tracking of the jet interface)

- IALOPT 10 1 (improved numerical robustness)

The Bromley correlation for film boiling has been assumed up to the cell row k=4, i.e. including the debris catcher.

With respect to jet break-up and drop fragmentation different parameter combinations have been tried but a really satisfactory recalculation of the experiment could not be found.

3.3.3 Standard jet break-up model

This model might also be called ‘parametrical model’ because it assumes constant prescribed mass removal rates (break-up) rates from the jet (per unit jet surface) and a constant size of the drops created in that process. It has been used with the option IOPT 16 1 invoking recent corrections.

Using the default values of all parameters in the jet break-up and the drop fragmentation models (case D2), the calculated pressure rise was very low. So, considering the relatively low melt jet velocity (< 3.5 m/sec up to 0.65 sec), the parameter SVITJET, i.e. the jet velocity below which the break-up rate is reduced to zero, was reduced from 2.0 to 0.5 (case D6). This has the desired effect but the pressure still remains too low, especially in the initial phase, see Figure 20. Please note that in the calculations, times are those of Figure 18 plus 0.32 sec.

The calculation completely fails to reproduce the steep pressure rise that follows the first steep pressure rise in the melt generator (0.3975…0.492 sec). Apparently the steep pressure rise in the interaction vessel (in the experiment) is a consequence of the increased melt exit velocity. So, it is not astonishing to see that the break-up model using constant break-up rates doesn’t reproduce this feature.

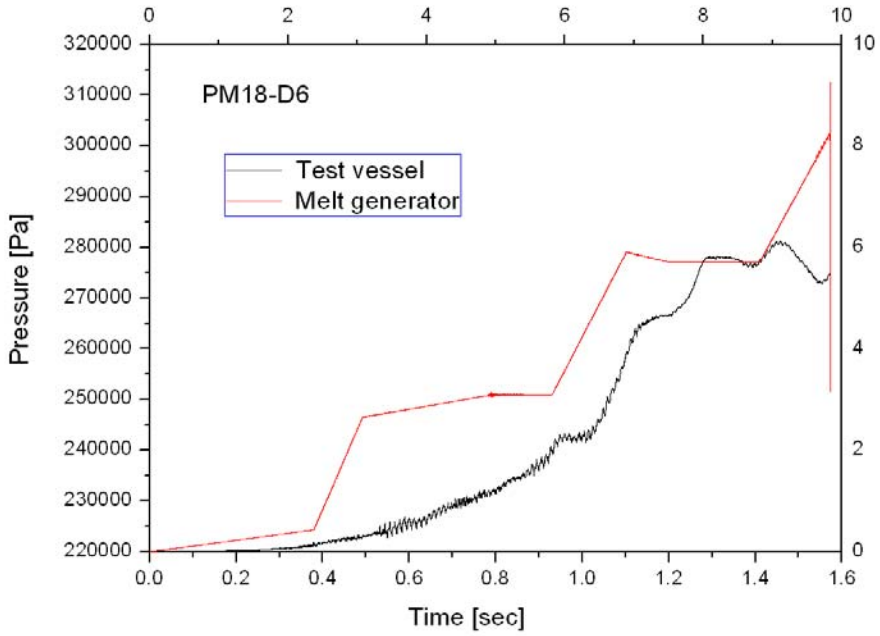

Figure 20: Gas pressure in the test vessel, calculated with the standard jet break-up model. The calculation is valid until blow-through occurs at 1.54 sec. The pressure in the melt generator is prescribed until 1.572 sec, i.e. except for the extremely fast changes in the end (>1.573 sec). The experimental results are shown in Figure 18. Mind the difference (shift) in time scales. At about 1.2 and 1.4 sec the calculation is close to the experiment.

In this calculation, the jet mass within the original pool area remains very small (less than 1 kg) while the drop mass increases to 11.9 kg. At 1.541 sec blow-through from the melt generator occurs. At this time, about 14.1 kg of melt have been released. This is about the correct melt mass but the average melt release rate has been about 20 % too high over most of the time (in spite of an assumed release diameter of 36 mm).

The Sauter mean diameter initially assumes the value of 4 mm corresponding to the prescribed size of drops torn from the jet. It later decreases roughly linearly to 3.35 mm. May be, that is the reason for the somewhat steeper pressure rise after about 1 sec, leading to values that are slightly too high.

3.3.4 Kelvin-Helmholtz (K-H) model of jet break-up

A scoping calculation (case F1) has been performed with both parameters, FRAGNUM and CDIACRE, set to 1. The default value for FRAGNUM, the multiplier to the break-up rate, however, is 3. CDIACRE is the ratio between the diameter of the particles torn from the jet and the K-H wave length. Its default value is 1. SVITJET (cf, 4.3.3) is set to 0.5. Whether this has an influence when

using the K-H model is not known. For drop fragmentation the default parameters are used.

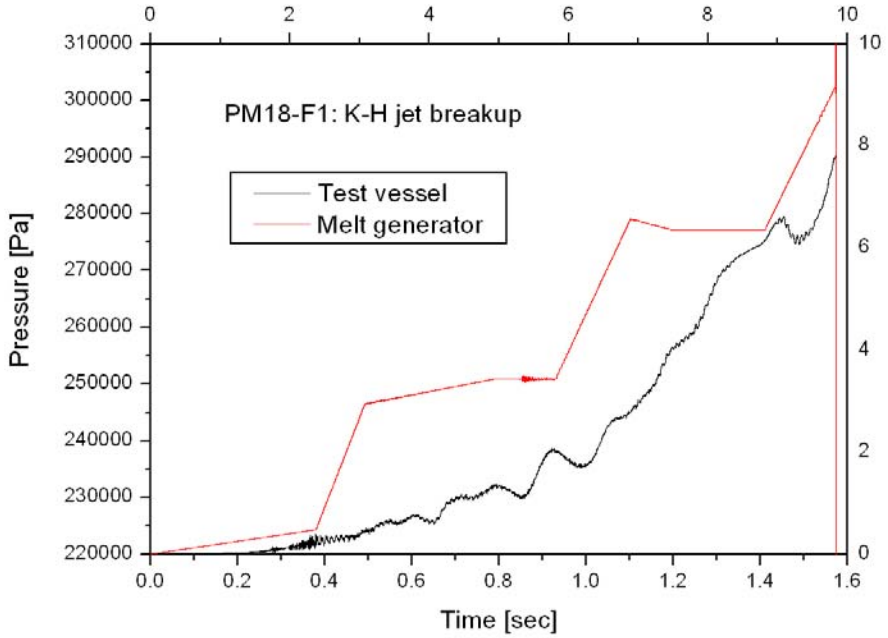

Figure 21: Gas pressure in the test vessel, calculated with the Kelvin-Helmholtz jet break-up model. The calculation is valid until blow-through occurs at 1.537 sec. The pressure in the melt generator is prescribed until 1.572 sec, i.e. except for the extremely fast changes in the end.

The calculated pressure history is shown in Figure 21. Towards the end, around 1.4 sec, the right level is reached but again the steep rise at 0.5 sec is missing. So, again the melt release rate is overestimated and blow-through occurs at 1.537 sec, when 15.2 kg have been released (the initial melt mass in the melt generator had been increased to 16.44 kg). So, the melt release rate is again too high by about 20 % which, of course, leads to higher pressures.

The Sauter mean diameter remains below 3.25 mm all the time. It decreases to about 2.75 mm between 1.1 and 1.3 sec, which might explain the steeper pressure rise after 1.1 sec.

In another calculation (F8), FRAGNUM, the multiplier to the break-up rate is set to 3. (the default value), but CDIACRE, the multiplier for the drop size is set to 1.33. The latter seems to dominate what is going on as the pressure in the vessel remains very low: < 0.235 MPa prior to the blow-through at 1.4 sec.

Melt drop fragmentation seems to be unimportant although the range for reducing the Weber number (APPRWE) has been reduced from its default value (20.) to 5.

The Sauter mean diameter ranges essentially between 10 mm initially and 7.5 mm in the end.

If, under otherwise the same assumptions, CDIACRE is reduced (case F9) to 0.5, the pressure grows more rapidly. But it remains too low initially and increases too much and too fast after 1.2 sec

If, under the conditions of the scoping calculation (FRAGNUM and CDIACRE, set to 1.), drop fragmentation is much increased by cutting the critical Weber number (WECRGOU) by two (to 6.) and using APPRWE = 5. (case F4), again about the right pressure level is reached in the end and one finds a possible correlation between increased jet velocity (due to increased driving pressure difference) and pressure increase, see Figure 22.

However, it seems impossible to correlate the steeper pressure rises occurring at about 1.0 and 1.4 sec with either a clear decrease in jet mass (jet break-up) or a significant decrease of the mean melt drop diameter (creation of smaller drops from the jet or drop fragmentation). The Sauter mean drop diameter, in this case, ranges essentially between 2.9 and (in the end) 2.5 mm.

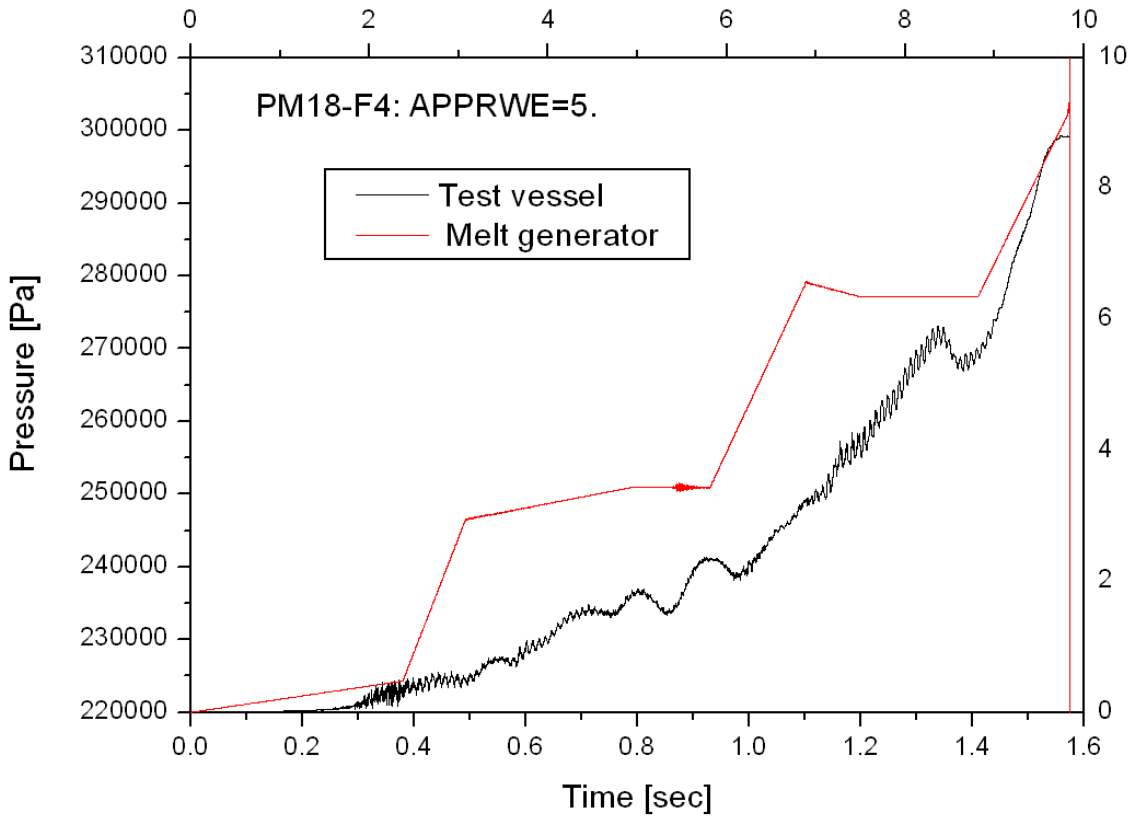

Figure 22: Gas pressure in the test vessel, calculated with the Kelvin-Helmholtz jet break-up model. The calculation is valid until blow-through occurs at 1.575 sec.

The pressure in the melt generator is prescribed until 1.572 sec, i.e. except for the extremely fast changes in the end (after the blow-through).

3.3.5 Considerations on the particle size spectrum

There seems to be a basic problem concerning the size distribution (particle size spectrum). After the experiment, 14.6 kg of Al_2O^3 have been recovered in the test vessel. Out of that, 5.7 kg had formed a cake in the debris catcher, the remainder was found in the shape of mostly round particles.

A small mass fraction (about 5 %) had diameters larger than 10 mm. Almost 50 % of the mass had diameters between 10 and 5 mm. That means that less than 50 % of the particles had diameters smaller than 5 mm.

However, in the three calculations that are shown here because the pressure at least towards the end reaches about the correct level, always most of the melt has already been released at 1.4 sec and at that time more than 97.6 % of the particles have diameters below 5 mm.

It was tried to enforce an early break-up of the jet into large drops by setting the fragmentation rates in the standard break-up model to high values, e.g. FRGVAP, the break-up rate in vapor to 0.1 $m^3/(sec*m^2)$ (default 0.001) and FRGFLM, the break-up rate in film boiling to values between 0.7 and 1.0 (default 0.1) while setting DIACRE, the initial drop diameter to 10 mm.

In all these cases, the complete break-up of the jet was readily achieved but the pressures remained very low because the drop diameters remained large. Even when the critical Weber number for drop fragmentation (WECRGOU) was set to 6. (and APPRWE to 5., case D16), the pressure rose only by about 0.01 MPa, i.e. by only 25 % of the experimental value until 1.1 sec, when the calculation failed because a too large pressure change occurred in one cell [probably in (5,1,5) in which the pressure was as low as 0.09 MPa].

In the end, 93 % of the released melt where in the form of drops but there was no melt drop with a diameter below 7.3 mm. So, the problem does not seem to be related with the jet break-up but with the fragmentation of the melt.

This conclusion is supported by the observation that very small drops are missing in these calculations: Only in case F4 (Figure 22), 7.4 % of the drops have a diameter between 1 and 2 mm. There are none with diameters below 1 mm. In the other two calculations even diameters below 2 mm are practically absent. This does not compare well with the experiment in which about 15 % of the mass was in drops with diameters below 2 mm and 2 % had diameters below 1 mm.

4. Conclusions

The most important finding of this study is that the intense heat transfer from hot particles (liquid or solid) to their highly agitated two-phase surrounding that forms when these particles are mixed with liquid water, cannot be described properly with the standard film boiling correlations like those of Epstein-Hauser, Liu-Theofanous or Bromley that are available in MC3D.

Only the correlation by Dhir-Purohit gives reasonable results. But even with Dhir-Purohit the steep pressure rise in the beginning of experiment QUEOS 58 cannot fully be reproduced. This could mean that even Dhir-Purohit underestimates the heat transfer or that condensation is overestimated during this phase with the parameters chosen in these calculations.

The bubble size model by Meignen (IOPT 76 1) which uses variable critical Weber numbers gives slightly better results in this phase but much worse results during the phase of steep pressure decrease. So, this model could not be used and condensation is essentially affected by setting upper and lower limits to the water drop and bubble diameters (the bubbles being more important).

It was tried to avoid unjustified values for these parameters. So the maximum diameters of both, drops and bubbles were set to 5 mm and essentially the smallest allowed diameter of the bubbles was used to fit the peak pressure in the calculation. This requires values in the range of 1…2 mm. The way, MC3D is set up, this value also applies to the drops.

Smaller drop diameters are not observed in these calculations. There is no physical argument for such a large minimum bubble size. But smaller values give wrong results because the bubble radius tends to assume either the maximum or the minimum allowed value. Therefore, also, the critical Weber number for bubble fragmentation has a very limited effect on condensation. All this means that the condensation could not really be controlled in these calculations. It could just be affected in a sufficient way.

During the pressure peak observed at the beginning of experiment QUEOS 58, high evaporation and condensation rates are calculated that nearly cancel each other. The maximum net evaporation rate is about one third of the maximum evaporation and condensation rates. That means that calculations of multiphase flows with intense heat transfer, as occur during premixing, are very sensitive to parameter variations affecting either evaporation or condensation, because the bottom line outcome results from a small difference between large numbers.

However, the high heat transfer rate proven by the QUEOS experiments (via the here performed analysis) also means that the melt interacting with the water during

premixing looses a lot of heat that is not available for conversion into work during a steam explosion that may occur later.

These heat losses may as well cool a lot of melt drops (especially the smaller ones) to such a degree that they have at least a frozen surface that prevents fine scale fragmentation during such explosion. In this way, these strong heat losses considerably reduce the explosion potential when a hot melt and water are intermixed.

In the calculations of the QUEOS experiment, heat conduction through the vapor film is by far the most important heat transfer mode. The next one, radiation to bulk water amounts to about one tenth of that. These relations remain about the same even if a sphere temperature of 3100 K is assumed: The only difference is that the heat transfer by radiation becomes slightly more important; it amounts to about one fifth of the heat conduction through the film.

It might seem surprising that the ‘standard’ film boiling correlations (which have been adjusted to experimental data) grossly underestimate the heat transfer in a cloud of hot particles (spheres or drops) falling through water. However, the situation there is largely different from single spheres within a well organized flow field.

The picture of single spheres surrounded by stable vapor films will apply at most to the leading ones. Behind them, the distorted flow through the particle cloud and the strong vapor generation will cause highly agitated, even chaotic motion of water and vapor around the spheres. This will lead to impingement of water globules on the surfaces of particles.

For very short times this will create direct contact between the hot material and liquid water so that a thin layer of water is superheated beyond the limit of stability (i.e. the spontaneous nucleation temperature) and evaporated explosively, creating new agitation of the flow field. This leads to extremely high heat transfer rates on small surface areas. Apparently the film boiling correlation due to Dhir and Purohit captures the effect of these processes although the underlying physics is quite different from normal film boiling.

The calculation results of QUEOS 58 indicate that of the hot spheres (or drops at that) that are ‘on flight’ through the water, the leading about 50 % are in a surrounding in which the gas volume fraction is similar to the hot particle volume fraction.

Only the trailing about 50 % are in an environment with large gas volume fraction. So, if the code should overestimate the void, this still would affect only half of the hot particles.

When analyzing premixing processes, one shouldn't look primarily on the absolute amount of void created but should analyze how much of the hot material is in areas with large void. As the transition from low void (similar to the hot particle volume fraction) to high void is very steep, one may consider hot particles surrounded by continuous water (according to the usual criterion of void less than 30 %) as those that can participate effectively in a steam explosion.

While the QUEOS experiment in which the heat transfer area is known can be reproduced quite well with MC3D, the recalculation of experiment PREMIX 18 which has been performed with a real melt and thus a melt surface area that develops in time proves to be more difficult and is less successful.

It is possible to obtain pressure increases of the right order with both jet break-up models available, the standard (parametric) model and the Kelvin-Helmholtz model when adjusting important parameters like SVITJET, the jet velocity below which the break-up rate is reduced to zero and the initial melt drop diameter (DIACRE and CDIACRE, respectively).

But in any case, the pressure rises too slowly in the beginning and has a tendency to suddenly increase too much in the end. The latter seems to indicate that one should not increase melt drop fragmentation beyond the parameter values used here (WECRGOU=6. and APPRWE=5.).

This seems to exclude a reasonable reproduction of the pressure history with a particle size spectrum corresponding to that found in the experiment, in which the largest mass fraction (almost 50 %) where in the diameter range 5 to 10 mm and less than 50 % had diameters below 5 mm.

Possibly the key to a better reproduction of both, the pressure history and the particle size spectrum lies in two types of melt drops being created from the melt stream which isn't necessarily a nice smooth jet: One could imagine that large drops (globules) are created by large-scale instabilities and Rayleigh-Taylor instability at and close to the tip of the stream, while small particles are created by (Kelvin-Helmholtz) surface instabilities along the sides of the melt stream.

One very general observation is made in the recalculations of both experiments: The measured pressure curves are normally quite smooth and show clear tendencies with few superimposed oscillations (i.e. local maxima and minima).

On the other hand, the calculated pressure curves are mostly quite undulated and even if there tendency (increasing or decreasing) is the same for some time, they show sudden changes in the steepness.

In other words: While the experiments give us elegant , nice and smooth curves, the calculations deliver us curves that suggest that the system doesn't really know

how to develop. Clear tendencies are marred by a lot of short-time variations. The latter might be due to local events that do not occur in this way in the experiments.

References

[1] J. Namiech, G. Berthoud, and N. Coutris, Fragmentation of a molten corium jet falling into water, *Nuclear Engineering and Design* **229** (2004) 265–287

[2] L. Meyer, G. Schumacher, H. Jacobs, and K. Thurnay, Investigation of the premixing phase of a steam explosion with hot spheres, *Nucl.Tech.,* **123**, 142-155 (1998)

[3] A L. Meyer, QUEOS Standard Tests for Code validation, unpublished report, Forschungszentrum Karlsruhe, April 1999
This summery report is available at http://nuklear-server.fzk.de/stresa_fzk/ For registration just follow the guide lines given there.

[4] A. Kaiser, W. Schütz, and H. Will, PREMIX experiments PM12-PM18 to Investigate the Mixing of a Hot Melt with Water, Scientific Report Forschungszentrum Karlsruhe, FZKA 6380, July 2001
This report is available at http://nuklear-server.fzk.de/stresa_fzk/

서 지 정 보 양 식			
수행기관보고서번호	위탁연구기관보고서번호	표준보고서번호	INIS 주제코드
KAERI/TR-3557/2008			

제 목 / 부 제	증기폭발 혼합계산의 최적모델 및 모델인자 결정
주 저 자	박익규 (열수력안전연구부)
공 저 자	김종환, 민병태, 홍성완

발행지	대 전	발행 기관	한국원자력연구소	발행일	2008년 3월
면 수	49p	도 표	유 (O), 무 ( )	크 기	A4

참고사항	2008' 중장기 연구 과제; 노심용융물 위해도 실증실험 및 쟁점해결기술개발		
비밀여부	공개 (O), 대외비 ( ), -----비밀	보고서종류	기술보고서
위탁연구기관	과학기술부	계약번호	

초 록

이 연구의 목적은 증기폭발의 혼합 계산에 있어서 가장 적절한 모델과 그 모델에 대한 모델 인자를 도출하는 것이다. 이를 위하여 Forschungszentrum Karlsruhe 에서 수행된 실험을 증기폭발 해석코드인 MC3D 에 적용하였다.

QUEOS 실험 결과가 혼합단계에서 가장 적절한 열전달 모델을 찾고 이 모델에 대한 모델상수를 도출하기 위하여 사용되었다. QUEOS 실험은 작고 뜨거운 고체구를 사용하였기 때문에 특히 열전달 모델에 대한 검토용으로서 적합하다. 고체구는 용융물과는 달리 열전달 면적이 고정되어 있기 때문에 열전달 모델에 대한 타당성 검토가 특히 유리하다.

QUEOS 실험을 사용하여 열전달 모델 및 모델 상수를 고정한 뒤에 PREMIX 실험을 사용하여 혼합계산을 다시 수행하였다. PREMIX 실험은 코륨의 상사물로서 용융된 알루미나(Al_2O_3) 를 사용한 혼합실험이다. PREMIX 실험을 통하여서는 용융물 제트와 용융물 drop 에 대한 용융물 분쇄 모델에 대한 검토가 이루어졌다.

주제명 키워드	혼합, 열전달, 용융물분쇄

BIBLIOGRAPHIC INFORMATION SHEET					
Performing Org. Report No.	Sponsoring Organization Report No.		Standard Report No.		INIS Subject Code
KAERI/TR-3557/2008					
Title/Subtitle	DETERMINATION OF APPROPRIATE MODELS AND PARAMETERS FOR PREMIXING				
Main Author	Ik-Kyu Park (Thermal Hydraulics Safety Research Center)				
Author	Jong-Hwan Kim, Beong-Tae Min, Seong-Wan Hong				
Pub. Place	Taejon	Pub. Org.	KAERI	Pub. Date	Febrary 2008
Page	49p	Fig. & Tab.	Yes (O), No ( )	Size	A4
Note	'2008 Nuclear Mid-Long Term Project				
Classified	Open (O), Outside ( ), ----- Class			Report Type	Technical Report
Sponsoring Org.	Ministry of Science & Technology			Contract No.	

Abstract

The purpose of the present work is to use experiments that have been performed at Forschungszentrum Karlsruhe during about the last ten years for determining the most appropriate models and parameters for premixing calculations.

The results of a QUEOS experiment are used to fix the parameters concerning heat transfer. The QUEOS experiments are especially suited for this purpose as they have been performed with small hot solid spheres. Therefore the area of heat exchange is known.

With the heat transfer parameters fixed in this way, a PREMIX experiment is recalculated. These experiments have been performed with molten alumina (Al_2O_3) as a simulant of corium. Its initial temperature is 2600 K. With these experiments the models and parameters for jet and drop break-up are tested.

Subject Keywords	Premixing, Heat Transfer, Break-up